Journal of Materials Chemistry C

ROYAL SOCIETY OF CHEMISTRY

PAPER

Check for updates

Quenching of persistent photocurrent in an oxide UV photodetector†

Baoshi Qiao, [ID] [ab] Zhenzhong Zhang,*[ac] Xiuhua Xie,[a] Binghui Li,[a] Xing Chen,[a] Haifeng Zhao,[a] Kewei Liu,[a] Lei Liu [ID][a] and Dezhen Shen*[a]

The sensitivity to weak light signals is a key parameter for UV photodetectors. However, a highly sensitive device has to suffer slow response speed (with photoconductive gain) or large noise current (with avalanche gain). In this work, a new type of photoconductive gain with controllable response speed is discovered in the Ga_2O_3 photodetector. The persistent photocurrent can be quenched by a 500 µs zero-voltage pulse. The photoconductive gain and the quenching of persistent photocurrent are respectively attributed to the forming and breaking of conductive filaments composed of oxygen vacancies. UV illumination has been demonstrated to accelerate the formation of the filament. This work provides a direction for the combination of speed-control and high sensitivity for photodiodes.

Introduction

UV photodetectors show numerous applications in space communication, missile and flame warning, ozone hole detection, *etc.*[1,2] Owing to the high photo sensitivity and high chemical stability, wide band-gap oxides attract more and more interest in UV detection materials.[3,4] Compared to commercial UV detectors like Si, photodetectors based on ZnMgO, Ga_2O_3 and $ZnGa_2O_4$ materials can work without optical filters and be used in a relatively extreme environment.[5,6] To sensitize the detection of weak UV signals, introducing a photoconductive gain is the most convenient route for a simple photodetector. However, it will slow down the response speed, and consequently limit their applications on high speed occasions.[7] The persistent photoconductivity (PPC) caused by long-lifetime carrier is considered as a main reason for the slow response time, which even lasts hours or days in oxide semiconductors.[8,9] This will cause the device to suffer from long dead-time, within which a second light pulse is not detected. If the PPC can be quenched controllably, the response speed can be tuned while the photocurrent is amplified, as realized in the gate-controlled three-terminal device.[10] Oxygen vacancy (V_O) and related defects are usually considered as the origin of PPC in oxides. They also play the

element of conductive filament in the memristor.[11,12] The migration of V_O in the memristor could be affected by illumination,[13–15] and amplification of current was realized in photoassisted memristors.[16] Russo *et al.* induced UV light into the ZnO memristor device. The density of V_O increases due to the desorption of oxygen under illumination and influences consequently the forming of the conductive filament. This leads to the multilevel current magnification of the memristor.[16] From another point of view, the persistent photocurrent may be controlled in an oxide-based photodetector containing abundant oxygen vacancies. However, the adsorption and desorption of oxygen at the ZnO surface is a slow process. Its further application as a photodetector is still restricted.[17–19] V_O also plays a leading role in Ga_2O_3 memristors.[20–22] Compared with ZnO material, the electric property of Ga_2O_3 is not so sensitive to oxygen (or air) at room temperature.[23,24] The above discoveries provide the possibility of PPC-current quenching in photodetectors with photoconductive gain.

In this work, a Ga_2O_3 UV detector with photo conductive gain based on a filament was fabricated. An obvious persistent photocurrent lasting hours or much longer could be quenched within several hundred microseconds by adding a 0 V pulse. Different from three-terminal devices, this quick recovery property is due to the breaking of the conductive filament and does not need gate control. This shows the enormous potential in speed controllable photodetection. On the other hand, this temporary storage of the illumination information can also be used in photoelectric memristors and visual memory simulation.

[a] State Key Laboratory of Luminescence and Applications, Changchun Institute of Optics, Fine Mechanics and Physics, Chinese Academy of Sciences, No. 3888 Dongnanhu Road, Changchun, 130033, People's Republic of China. E-mail: shendz@ciomp.ac.cn

[b] University of the Chinese Academy of Sciences, Beijing 100049, People's Republic of China

[c] School of Microelectronics, Dalian University of Technology, Dalian, Liaoning 116024, People's Republic of China. E-mail: zhangzz@dlut.edu.cn

† Electronic supplementary information (ESI) available: SEM, AFM, XRD, PL, and speed-measurement diagram. See DOI: 10.1039/d0tc05997h

Experimental

The Ga_2O_3 thin film was grown on a Si/Al_2O_3 substrate by low-pressure metalorganic chemical vapor deposition (LP-MOCVD)

This journal is © The Royal Society of Chemistry 2021

J. Mater. Chem. C, 2021, **9**, 4039–4045 | **4039**

method. Si(111) was used as the substrate, which experienced ultrasonic bathing in trichloro ethylene, acetone, ethyl alcohol and deionized water, respectively. Trimethylgallium (TMGa) and 5-N O_2 were used as the precursors and the carrier gas was 6-N nitrogen evaporated from liquid nitrogen. The growth temperature was kept at 650 °C, and the chamber pressure was held at 500 Pa. The flow rate of the Ga source was 5 SCCM (standard-state cubic centimetre per minute). The oxygen flow rates for the thin films with high and low V_O density were 120 SCCM and 1000 SCCM, respectively. In order to promote the nucleation of the Ga_2O_3 thin film, an Al_2O_3 buffer layer was pre-deposited by the atomic layer deposition (ALD) method, which is used to ensure an acceptable crystal quality. The growth lasted 30 cycles at a deposition temperature of 200 °C. The thickness is estimated to be 3 nm according to the cycle number. Trimethylaluminum and H_2O were used as the precursors with an action time of 40 ms and 60 ms, respectively.

The morphology and structure of the Ga_2O_3 films were characterized by scanning electron microscopy (HITACHI S-4800) and X-ray diffraction (Bruker D8GADDS) with Cu Kα radiation (λ = 0.154 nm), respectively. The surface roughness is characterized by an atomic force microscope (BRUKER MULTI-MODE 8). The electrical characteristics were measured on a semiconductor device analyzer (Agilent B1500A). The spectral response was measured using a responsivity measurement system equipped with an SR 830 lock-in amplifier and a 150 W Xe lamp. The time resolution response was recorded

by a Tektronics DPO5104 oscilloscope using a 254 nm portable UV analyzer. The pulse voltage was provided by a precision source (Agilent B2902A).

Results and discussion

The Ga_2O_3 thin film is composed of dense grains, and the thickness is about 330 nm, as shown by the SEM images in Fig. S1 (see ESI†). The Al_2O_3 buffer layer is hardly observed due to its small thickness of about 3 nm. The atomic force microscopy image is shown in Fig. S2 (ESI†). The root-mean-square surface roughness of the Ga_2O_3 thin film is 13.3 nm. The X-ray Diffraction characterization indicates that the Ga_2O_3 is crystallized in the pure beta phase. Except for the diffraction peak of the Si[111] substrate, the other diffraction peaks come from β-Ga_2O_3 (see Fig. S3, ESI†).

Fig. 1a shows the *I–V* curve in linear-coordinates. Indium and copper electrodes were fabricated on the Ga_2O_3 surface and the backside of the Si substrate, respectively. The inset sketches the structure of the device. The *I–V* curves with symmetrical electrodes are shown in Fig. 1b, confirming a good ohmic contact between the thin film and electrode. It can be inferred that the rectifying characteristic comes from the Ga_2O_3/Si heterojunction. The rectification ratio is larger than 2 orders of magnitude. In this work, the forward bias on the heterojunction is defined as the situation that positive bias is applied
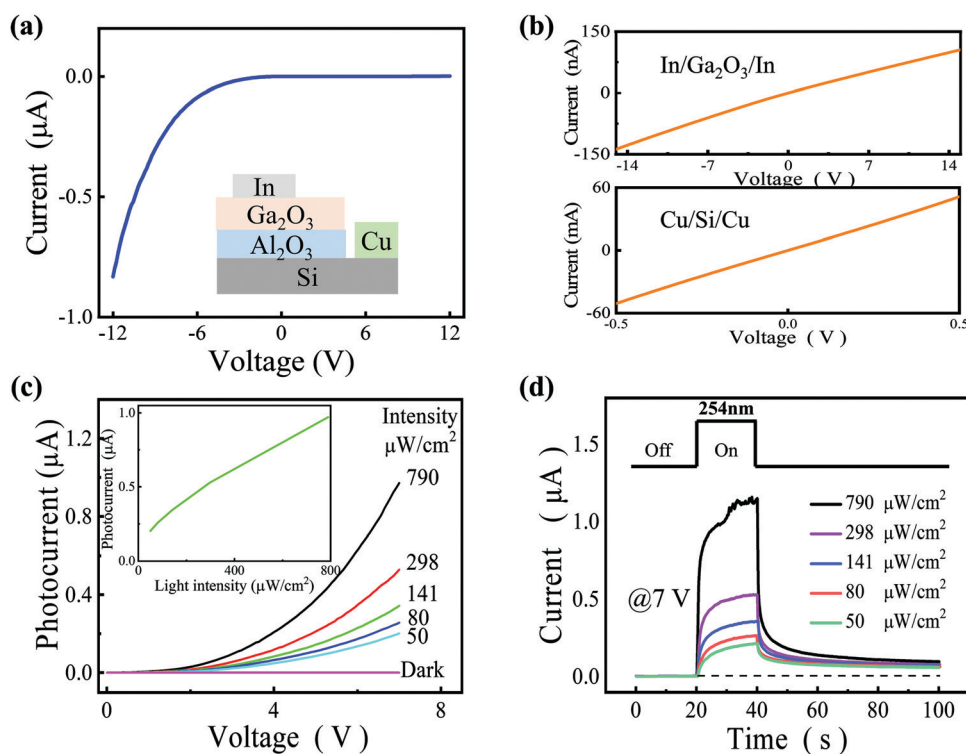

Fig. 1 (a) The *I–V* curve. The inset is the structure of the Si–Ga_2O_3 device. (b) The *I–V* curves of the electrode contact. (c) The photocurrent *vs.* bias voltage under different illumination intensities. The inset shows the change of photocurrent at 7 V *vs.* illumination intensity. (d) The *I–t* curves at 7 V under different illumination intensities. The illumination light operation is shown by the black line in the upper part.

4040 | *J. Mater. Chem. C*, 2021, **9**, 4039–4045

This journal is © The Royal Society of Chemistry 2021

on the indium electrode. Fig. 1c shows the I–V curves measured under 254 nm illuminations with different light intensities. The Ga_2O_3 thin film in this work exhibits sensitivity toward UVC. The maximum responsivity is calculated to be 1.2 A W^{-1} by[25,26]

$$R = (I_{ph} - I_d)/\rho S \qquad (1)$$

The I_{ph} and I_d are the photocurrent and dark current respectively, ρ is the light intensity and S is the efficient illumination area, which is 0.1 mm^2. The quantum efficiency is 586%, indicating the presence of inner gain. The photocurrent at 7 V vs. illumination intensity is shown in the inset. The photocurrent shows a super-linear increase with the bias-voltage, and a near linear increase with the illumination intensity. Similar to many Ga_2O_3 based UV detectors, this device also shows a certain PPC characteristic.[27,28] Fig. 1d depicts the I–t curves under 254 nm illumination with different power densities. The device shows a long-time current decay after illumination. Even for an illumination density as low as 52 μW cm^{-2}, the current in the dark remains 64 nA at 40 s after shutting illumination, which is hundreds of times larger than the dark current in Fig. 1a.

The PPC current is commonly believed to be caused by long-lifetime of the non-equilibrium carrier. It is closely related to deep-level defects.[29,30] Oxygen vacancies are the most common defect in oxides. They may be responsible for the PPC in this work. To support the above conjecture, the photoelectrical properties of Ga_2O_3 thin films with high and low V_O density are studied. The difference in V_O density was supported by room-temperature photoluminescence (PL) spectra, as shown in Fig. S4 (ESI†). Fig. 2a shows the I–t curves of the samples with high and low V_O density. The 254 nm light turns on at time 20 s and off at 40 s. In the case of high V_O density, the photocurrent is significantly larger than that with low V_O density. This supports that the PPC current is caused by V_O and the consequential inner gain. In an unintentionally doped Ga_2O_3 thin film, V_O can be generated in the internal of the film during the growth or on the surface by adsorption and desorption of oxygen molecules.[27] Both of the two origins will lead to a PPC current. In general, there is an obvious difference between the two types of V_O defects. To clarify the main origin of the V_O defects, the I–t curves were measured in a vacuum and air atmosphere, as shown in the inset in Fig. 2a. No obvious
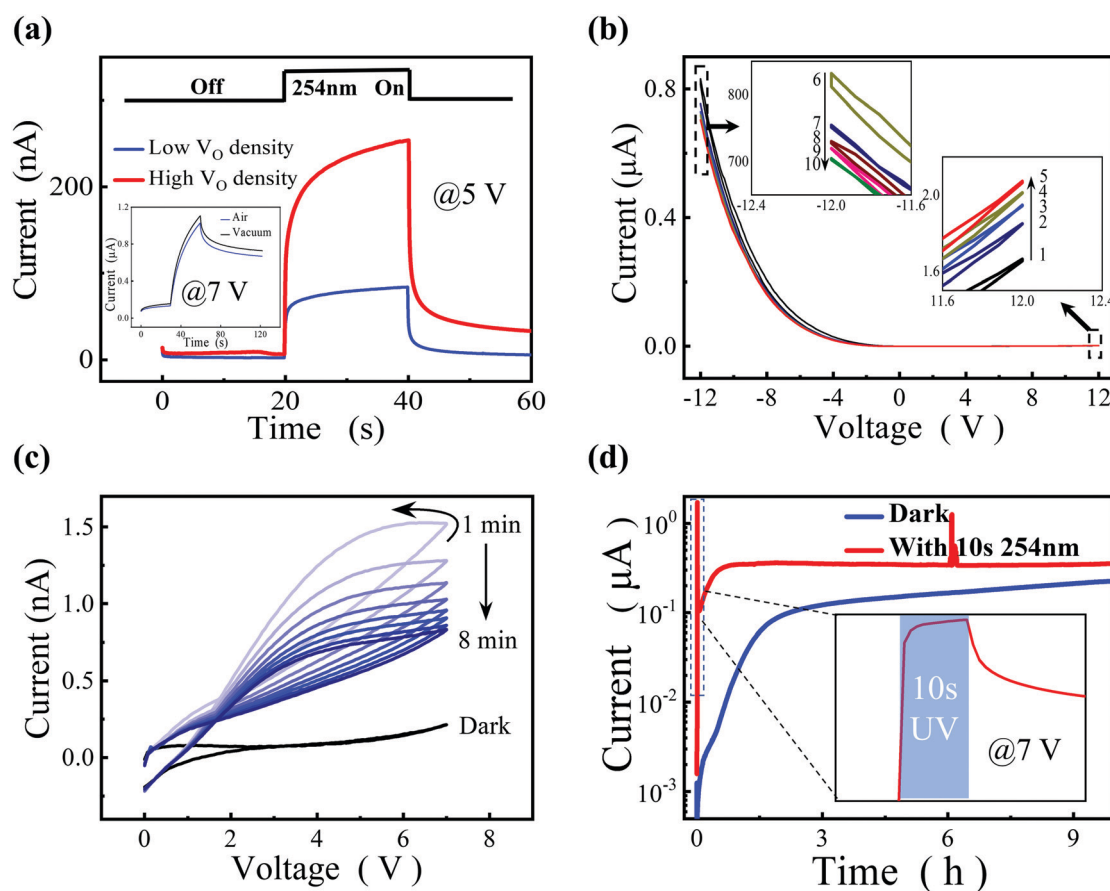

Fig. 2 (a) The I–t curves of devices with high and low V_O density under 254 nm illumination, where the illumination intensity is 790 μW cm^{-2}, and the bias is 5 V. The inset shows the I–t curves of the device in a vacuum and air atmosphere. (b) The cyclic I–V scanning in the dark without any pre-illumination. The scanning is performed cyclically under positive bias 5 times and then in negative bias 5 times. The inset shows the details near ±12 V. (c) The cyclic I–V scanning in the dark after 254 nm pre-illumination. The dark current without any pre-illumination is also shown here, as depicted by the black curve. (d) The long-time current measurement without and with 10 s UV pre-illumination in semi-log coordinate. The inset shows the details during pre-illumination.

change is observed between the two cases. This suggests that the V_O defects come from the interior of the thin-film, not the surface.

As mentioned in reports on memristors, the V_O can migrate in an applied electric field, and influence the electrical properties consequently. Fig. 2b shows the cyclic scanning of the I–V curves in the dark. With the scan repeating, the forward current increases and the reverse current decreases. This feature is in accordance with the memory enhancing effect of some resistive switching devices.[31,32] The combined effect by illumination and electric field is studied through cyclic scanning I–V tests at different times after shutting the 254 nm illumination, as shown in Fig. 2c. The power density is 790 μW cm^{-2}. At one minute after shutting the UV illumination, the dark current at 7 V is 1.5 nA. With cyclic scanning in 8 min, it gradually decreases to 0.83 nA. Furthermore, the I–V curves in this work show a significant hysteresis loop feature during the cyclic scanning. In general, the anticlockwise and clockwise I–V hysteresis is related to memristivity and charge–discharge of a capacitor, respectively.[33,34] That is, the device shows the memristive feature at high voltage and the discharge character at low voltage. It is found that the loop feature weakens

gradually with time after pre-illumination. It can be deduced that the memristive feature is closely related to illumination. As is well-known, only charged oxygen vacancies (V_O^+) can be driven by the electric field. Under 254 nm illumination, the V_O can quickly transform into V_O^+ by trapping a photogenerated hole. The V_O^+ defects can gather near the negative electrode, and form a conductive filament under an electric field. As a result, a PPC current is introduced, as observed in Fig. 1d.

To study further the illumination influence on the PPC current process, long-time evolvements of current in the dark with/without pre-illumination are shown in Fig. 2d. The current in the dark without pre-illumination shows a gradual increase in the first 90 min and tends to saturation. For the case with 10 s pre-illumination, the above process is completed within 30 min. This indicates that the UV illumination is an effective accelerator of this process. In a semi-insulating Ga_2O_3, the V_O^+ is hard to be formed in the dark. Very few V_O^+ defects are gathered near the electrode to form a filament. Under illumination, abundant electrons and holes are generated. Therefore, numerous V_O^+ defects are produced by trapping holes and move toward the negative electrode. Near the negative electrode, the V_O^+ defects are gathered and restored, acting as the
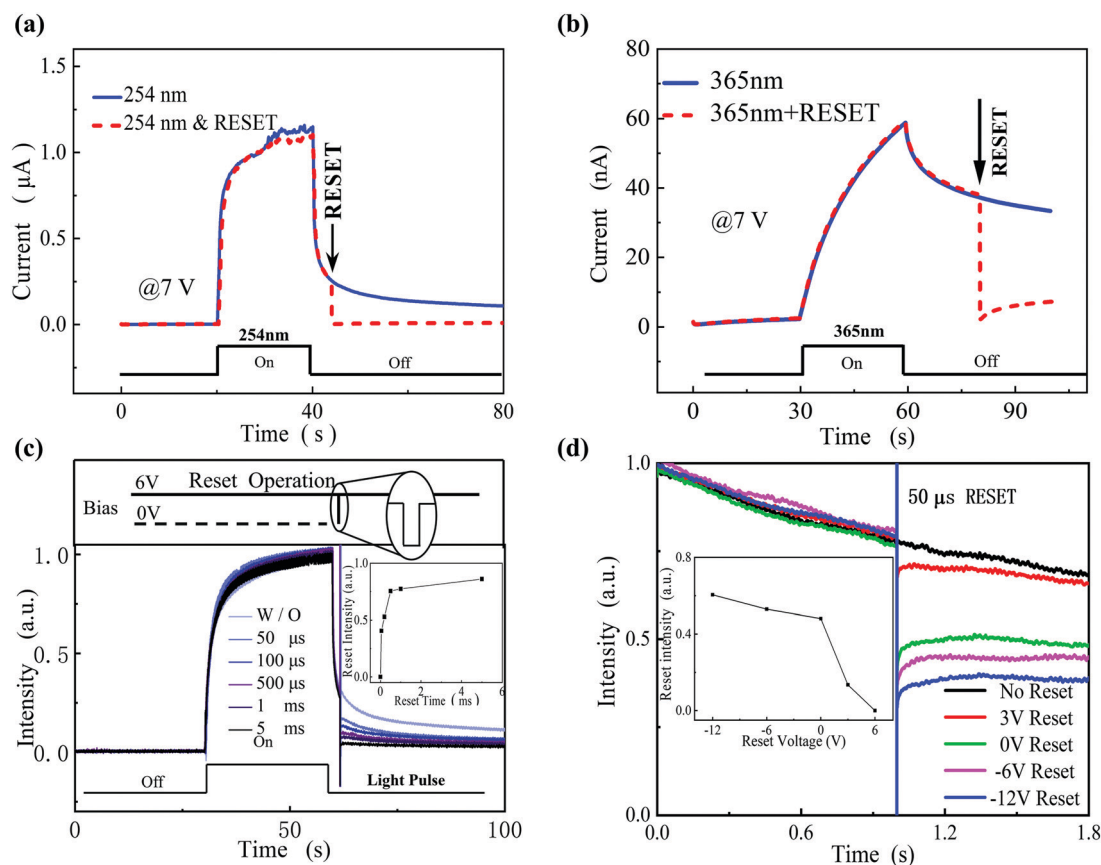

Fig. 3 The I–t curves under (a) 254 nm and (b) 365 nm illumination with/without the 0 V-pulse resets. The illumination light operation is shown by the black line at the lower part. The 0 V pulse is applied at the time of reset. (c) The reset effects with different pulse widths. The illumination operation is described by the black line at the lower part. The bias and reset operations are shown in the upper part. The inset shows the reset intensity vs. reset pulse width. (d) The evolvement of PPC after resetting with different voltage, where the pulse width is fixed at 50 μs. The reset intensity vs. reset voltage is shown in the inset.

4042 | J. Mater. Chem. C, 2021, 9, 4039–4045

This journal is © The Royal Society of Chemistry 2021

extension of the electrode. Namely, the negative electrode is extended toward the positive electrode. It is found that the current after pre-illumination decreases within the first 200 s and then increases. This indicates that the decrease of resistivity is not caused by the reduction of barrier height near the junction, which leads to a monotonic change. That is, the current evolvement is in accordance with the formation process of the conductive filament based on the migration of the V_O^+ defect. At the beginning of the test, the electric field in the thin film is relatively uniform. Under illumination, abundant V_O defects gather near the negative electrode and begin to form a multi-conductive filament. Once one of the filaments starts to dominate, others are inhibited and disappear gradually with the electric field weakening, which will lead to a decay of PPC. Finally, after a relatively long time, the surviving conductive filament extends and undertakes most of the current.

Since the PPC is caused by the V_O^+ defect, it should be controlled by the applied electric field, as in some memristors. As shown by the red line in Fig. 3a, the PPC current is reset to a markedly low level by removing temporarily the electric field, *i.e.* adding a 0 V pulse. After the reset, the PPC current is decreased from 257 nA to 4.5 nA. The device is turned into a high resistant state. In fact, the change of resistance has been found in the hysteresis curve, as reflected by the intersection of the loop at low voltage in Fig. 2c. This means the dispersion of V_O^+ defects at a low electric field, which results in the breaking of the conductive filament. Besides the case under 254 nm illumination, the PPC and reset behavior are also observed under 365 nm illumination, as shown by Fig. 3b. In general, the V_O^+ can be formed through V_O trapping holes generated by interband excitation. Moreover, V_O can become V_O^+ by ionizing an electron onto the conduction band under intraband excitation. The spectral response of the $Si/Al_2O_3/Ga_2O_3$ device is shown in Fig. S5 (ESI†). The −3 dB cutoff is at about 260 nm. However, the reject ratio (R_{250nm}/R_{280nm}) is only 20.8, indicating a poor selectivity in the spectral response of the device. It can be found that the device also possesses a low response at the near UV band. This is caused by intraband excitation.

The dynamics of V_O (V_O^+) play a key role in the PPC and its quenching. Therefore, the reset effect is markedly influenced by the width and voltage of the reset pulse. An oscilloscope was used to assist in the characterizing of the reset behavior. The measurement configuration is shown in Fig. S6 in the ESI.† The sampling resistor is 200 kohm, which is much smaller than the resistance of the device either in the dark or under illumination. Fig. 3c shows the influence of pulse width of the 0 V reset pulse on the quenching of the PPC current. The reset intensity dependence on the width of the 0 V pulse is shown visually in the inset. With widening the reset pulse, the PPC current decreases monotonously, and the attenuation tends to be constant. It can be found that the pulse with a width larger than 500 μs can realize a significant quenching effect. Fig. 3d shows the effect of the electric field on the reset effect. The width of the pulse voltage is fixed at 50 μs. The reset intensity is enhanced continually by decreasing the pulse voltage from 3 V to −12 V, reflecting the influence of V_O^+ drift on the resetting process. The inset in Fig. 3d shows the reset intensity dependence on the reset voltage. It could be found that the change mostly locates in the bias range of 0–3 V. This means that such a low electric field cannot maintain the filament and most V_O^+ defects depart from the negative electrode.

In fact, an avalanche photodiode working in Geiger mode possesses a similar reset function. However, it cannot reflect the illumination intensity, and cannot be reset to different levels controllably by changing the voltage of the reset pulse. Besides, an avalanche photodiode has to suffer from random noise because of the randomness of impact ionization. The device in this work has no disadvantages mentioned above.

The schematic diagram for the forming and breaking of conductive filaments is shown in Fig. 4, where the conductance evolvement is sketched using a blue curve. The V_O defects
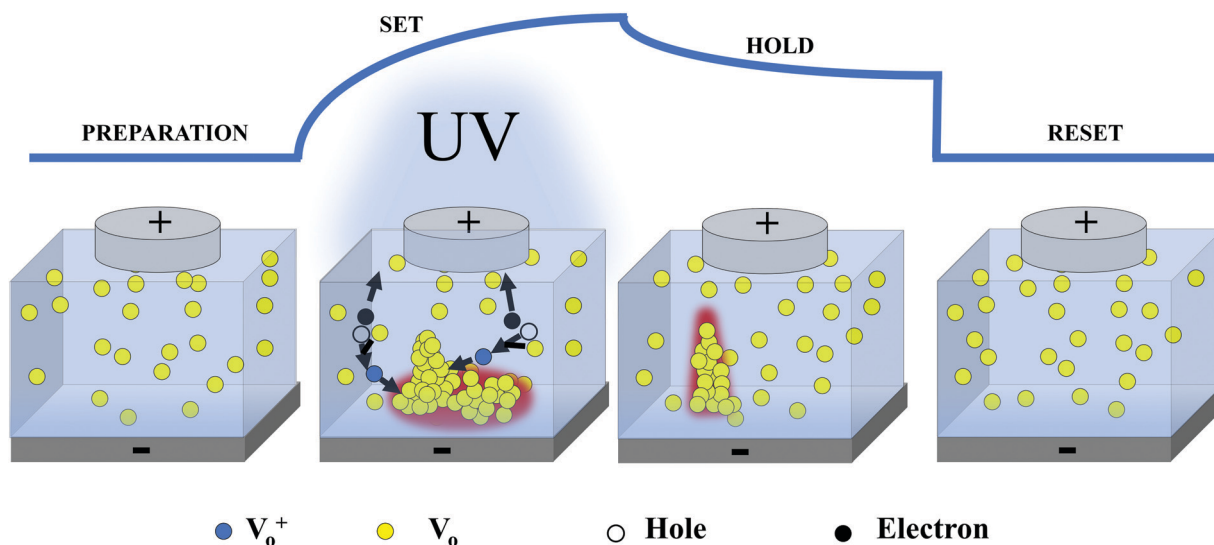

Fig. 4 The schematic of the formation and quenching of the conductive filament at different stages. The upper blue curve sketches the change of conductance of the device.

This journal is © The Royal Society of Chemistry 2021

J. Mater. Chem. C, 2021, **9**, 4039–4045 | **4043**

distribute randomly in the Ga_2O_3 materials before illumination, as shown in the preparation stage. When the device is illuminated by 254 nm light, the electrons and holes are generated and participate in the conduction under an electric field. Some V_O defects trap the holes and become V_O^+. The V_O^+ defects migrate to the negative electrode and are gathered there. The abundant V_O^+ defects near the negative electrode act as the extension of the electrode. Finally, a conductive filament forms in the Ga_2O_3 thin film, as shown in the set stage. Once one conductive filament composed of V_O is formed, the electric field between the filament tip and the positive electrode will be strongest, and the formation of other filaments is inhibited naturally. In the hold stage, the illumination is off. The photo-generated carriers recombine quickly and the V_O^+ decreases consequently. But the conductive filament still remains, as shown by the third diagram. The behavior of PPC current comes from the competition between recombination of carriers and the growth of the conductive filament. In the reset stage, because the electric field is absent for a short time, the V_O^+ defects on the filament diffuse in the thin film under the driving of Coulomb repulsion and concentration difference. As a result, the conductive filament dissipates and the PPC current is quenched.

Conclusions

To summarize, a UV detector with a new type of inner gain based on a Ga_2O_3 thin film was fabricated. The persistent photocurrent caused by the gain can be tuned by adding a 0 V pulse. The PPC current and its quenching are attributed to the forming and breaking of the conductive filament composed of oxygen vacancies. The formation and survival of the conductive filament depends on the electric field and is affected significantly by the UV illumination. The conductive filament shows huge potential in magnifying the photocurrent. This speed controllable UV detector shows prospects in UV vision and UV information storage.

Author contributions

This manuscript was written through the contributions of all authors. All authors have given approval to the final version of the manuscript.

Conflicts of interest

There are no conflicts to declare.

Acknowledgements

References

1 R. Yu, G. Wang, Y. Shao, Y. Wu, S. Wang, G. Lian, B. Zhang, H. Hu, L. Liu, L. Zhang and X. Hao, *J. Mater. Chem. C*, 2019, **7**, 14116.

2 X. Chen, K. Liu, Z. Zhang, C. Wang, B. Li, H. Zhao, D. Zhao and D. Shen, *ACS Appl. Mater. Interfaces*, 2016, **8**, 4185.

3 F. Alema, B. Hertog, O. Ledyaev, D. Volovik, G. Thoma, R. Miller, A. Osinsky, P. Mukhopadhyay, S. Bakhshi, H. Ali and W. V. Schoenfeld, *Phys. Status Solidi A*, 2017, **214**, 1600688.

4 W. Y. Kong, G. A. Wu, K. Y. Wang, T. F. Zhang, Y. F. Zou, D. D. Wang and L. B. Luo, *Adv. Mater.*, 2016, **28**, 10725.

5 R. Lin, W. Zheng, D. Zhang, Z. Zhang, Q. Liao, L. Yang and F. Huang, *ACS Appl. Mater. Interfaces*, 2018, **10**, 22419.

6 M. Bosi, P. Mazzolini, L. Seravalli and R. Fornari, *J. Mater. Chem. C*, 2020, **8**, 10975.

7 D. Guo, Z. Wu, P. Li, Y. An, H. Liu, X. Guo, H. Yan, G. Wang, C. Sun, L. Li and W. Tang, *Opt. Mater. Express*, 2014, **4**, 1067.

8 K. Liu, M. Sakurai, M. Aono and D. Shen, *Adv. Funct. Mater.*, 2015, **25**, 3157.

9 H. T. Zhou, L. J. Cong, J. G. Ma, B. S. Li, M. Z. Chen, H. Y. Xu and Y. C. Liu, *J. Mater. Chem. C*, 2019, **7**, 13149.

10 S. Jeon, S. E. Ahn, I. Song, C. J. Kim, U. I. Chung, E. Lee, I. Yoo, A. Nathan, S. Lee, J. Robertson and K. Kim, *Nat. Mater.*, 2012, **11**, 301.

11 W. Xue, G. Liu, Z. Zhong, Y. Dai, J. Shang, Y. Liu, H. Yang, X. Yi, H. Tan, L. Pan, S. Gao, J. Ding, X.-H. Xu and R.-W. Li, *Adv. Mater.*, 2017, **29**, 1702162.

12 S. U. Sharath, S. Vogel, L. Molina-Luna, E. Hildebrandt, C. Wenger, J. Kurian, M. Duerrschnabel, T. Niermann, G. Niu, P. Calka, M. Lehmann, H.-J. Kleebe, T. Schroeder and L. Alff, *Adv. Funct. Mater.*, 2017, **27**, 1700432.

13 J. J. Yang, D. B. Strukov and D. R. Stewart, *Nat. Nanotechnol.*, 2013, **8**, 13.

14 W. Lu, J. Xiao, L. M. Wong, S. Wang and K. Zeng, *ACS Appl. Mater. Interfaces*, 2018, **10**, 8092.

15 J. Y. Mao, L. Zhou, X. Zhu, Y. Zhou and S. T. Han, *Adv. Opt. Mater.*, 2019, **7**, 1900766.

16 P. Russo, M. Xiao, R. Liang and N. Y. Zhou, *Adv. Funct. Mater.*, 2018, **28**, 1706230.

17 Z. Chen, B. Li, X. Mo, S. Li, J. Wen, H. Lei, Z. Zhu, G. Yang, P. Gui, F. Yao and G. Fang, *Appl. Phys. Lett.*, 2017, **110**, 123504.

18 D. Shao, M. Yu, H. Sun, T. Hu, J. Lian and S. Sawyer, *Nanoscale*, 2013, **5**, 3664.

19 R. Bo, N. Nasiri, H. Chen, D. Caputo, L. Fu and A. Tricoli, *ACS Appl. Mater. Interfaces*, 2017, **9**, 2606.

20 C. W. Hsu and L. J. Chou, *Nano Lett.*, 2012, **12**, 4247.

21 D. Y. Guo, Z. P. Wu, Y. H. An, P. G. Li, P. C. Wang, X. L. Chu, X. C. Guo, Y. S. Zhi, M. Lei, L. H. Li and W. H. Tang, *Appl. Phys. Lett.*, 2015, **106**, 042105.

4044 | *J. Mater. Chem. C*, 2021, **9**, 4039–4045

This journal is © The Royal Society of Chemistry 2021

22 J. J. Xu, W. Zheng and F. Huang, *J. Mater. Chem. C*, 2019, **7**, 8753.

23 Z. Liu, T. Yamazaki, Y. Shen, T. Kikuta, N. Nakatani and Y. Li, *Sens. Actuators, B*, 2008, **129**, 666.

24 T. Schwebel, M. Fleischer and H. Meixner, *Sens. Actuators, B*, 2000, **65**, 176.

25 C. Xie, P. You, Z. Liu, L. Li and F. Yan, *Light: Sci. Appl.*, 2017, **6**, e17023.

26 S. W. Shin, K. H. Lee, J. S. Park and S. J. Kang, *ACS Appl. Mater. Interfaces*, 2015, **7**, 19666.

27 S. Cui, Z. Mei, Y. Zhang, H. Liang and X. Du, *Adv. Opt. Mater.*, 2017, **5**, 1700454.

28 Y. Kwon, G. Lee, S. Oh, J. Kim, S. J. Pearton and F. Ren, *Appl. Phys. Lett.*, 2017, **110**, 131901.

29 Q. Hou, X. Wang, H. Xiao, C. Wang, C. Yang, H. Yin, Q. Deng, J. Li, Z. Wang and X. Hou, *Appl. Phys. Lett.*, 2011, **98**, 102104.

30 J. Xu, D. You, Y. Tang, Y. Kang, X. Li, X. Li and H. Gong, *Appl. Phys. Lett.*, 2006, **88**, 072106.

31 D. S. Jeong, H. Schroeder and R. Waser, *Nanotechnology*, 2009, **20**, 375201.

32 J. J. Yang, J. Borghetti, D. Murphy, D. R. Stewart and R. S. Williams, *Adv. Mater.*, 2009, **21**, 3754.

33 X. Zhao, Z. Wang, W. Li, S. Sun, H. Xu, P. Zhou, J. Xu, Y. Lin and Y. Liu, *Adv. Funct. Mater.*, 2020, **30**, 1910151.

34 Z. T. Xu, K. J. Jin, L. Gu, Y. L. Jin, C. Ge, C. Wang, H. Z. Guo, H. B. Lu, R. Q. Zhao and G. Z. Yang, *Small*, 2012, **8**, 1279.

This journal is © The Royal Society of Chemistry 2021

J. Mater. Chem. C, 2021, **9**, 4039–4045 | **4045**